Supporting Information

Engineering spinel $NiMgAlO_x$ catalyst derived from in-situ confined Ni into MgAl-LDH for hydrogen production via ammonia decomposition

Kai Hu[a,b], Fang Dong [a]*, Xiuzi He[a,b], Weiliang Han[a], Zhicheng Tang[a]*

(a. National Engineering Research Center for Fine Petrochemical Intermediates, State Key Laboratory of Low Carbon Catalysis and Carbon Dioxide Utilization, Lanzhou Institute of Chemical Physics, Chinese Academy of Sciences, Lanzhou 730000, China.

b. University of Chinese Academy of Sciences, Beijing 100039, China.)

S1. Chemical reagents

The chemical reagents used in this study included nitric acid (HNO_3), urea ($CO(NH_2)_2$), nickel nitrate hexahydrate ($Ni(NO_3)_2 \cdot 6H_2O$), magnesium nitrate hexahydrate ($Mg(NO_3)_2 \cdot 6H_2O$), aluminum nitrate nonahydrate ($Al(NO_3)_3 \cdot 9H_2O$) and deionized water. All reagents were of analytical purity (AR) grade and were used without further purification.

S2. Catalyst characterizations

The catalyst's surface area, pore volume and pore size were determined using nitrogen adsorption isotherms measured at -196 °C with an ASAP 2010 instrument (Micrometrics). The surface area and pore size distribution were then calculated using the Brunauer-Emmett-Teller (BET) and Barrett-Joyner-Halenda (BJH) methods, respectively. Prior to measurement, all samples were degassed in a vacuum at 300 °C for three hours.

Simultaneous thermal analysis (TG-DSC/DTA) was used to thermally decompose the sample. The sample was heated to 800 °C in air at a rate of 10 °C per minute, and the change in mass during this process was recorded.

The crystalline phase of the catalyst was analyzed by X-ray diffraction (XRD). This analysis was conducted using a Japan SmartLab diffractometer with Cu Kα radiation (λ=1.5406 nm). The scanning was performed at 10°-90°, with a scanning speed of 0.5°/min, at 60 kV and 55 mA.

X-ray photoelectron spectroscopy (XPS) measurements were conducted using a Thermo Scientific 250 Xi spectrometer. The binding energies were calibrated to the C 1s peak at 284.8 eV.

The microstructure of the catalyst was observed using transmission electron microscopy (TEM) with a JEOL-JEM-2010 instrument. The elemental distributions of Ni, Mg, Al and O were analyzed by means of energy dispersive X-ray spectroscopy (EDXS) in conjunction with TEM.

The experiment employs the TP-5080-D fully automatic multi-function adsorption instrument (manufactured by Xianquan Co., Ltd.), equipped with a double-walled quartz reactor. In order to guarantee both gas tightness and stability, it is imperative that the reactor is connected to the gas pipeline at both extremities. This is achieved by means of high-precision Swagelok connectors. The temperature of the reactor is meticulously regulated by an external heater, with synchronized real-time data on temperature and thermal conductivity detector (TCD) signals being recorded by the data acquisition system.

For H_2-TPR, 50 mg of the catalyst underwent a pretreatment in He at 300 °C for a duration of one hour, followed by cooling to 40 °C. Subsequent to the TCD baseline stabilization, the gas was transitioned to a 10% H_2/N_2 mixture (40 mL/min), and the sample was heated to 900 °C at a rate of 10 °C/min.

For N_2-TPD, 50 mg of the catalyst was first pretreated under H_2 flow at 500 °C for 2 hours, followed by cooling to 40 °C and exposure to pure N_2 for 1 hour to allow nitrogen adsorption. Subsequently, the gas was transitioned to He, and once the TCD

baseline had been stabilized, the sample was heated to 900 °C at a ramp rate of 10 °C/min.

For the NH_3-TPD sample, 50 mg of the catalyst in He at 300 °C for one hour was conducted to remove surface impurities and moisture. Following this, the sample was cooled to 40 °C. A gas mixture comprising 10% NH_3 and N_2 was introduced for a duration of one hour, with the objective of achieving NH_3 adsorption. Following purging with He and stabilizing the TCD signal, the sample was heated to 900 °C at a rate of 10 °C /min.

For the CO_2-TPD study, 50 mg of the catalyst was treated under N_2 by heating from room temperature to 300 °C at a rate of 10 °C/min, after which a holding period of one hour was implemented. Following a period of cooling to room temperature, a 5% CO_2/N_2 mixture was introduced, and the sample was heated to 50 °C and held for 1 hour to ensure CO_2 adsorption. During this step, N_2 flow was maintained. Subsequently, the temperature was increased to 900 °C at a rate of 10 °C/min for desorption.

The surface reaction behavior of the catalyst was characterized by in-situ diffuse reflectance infrared Fourier transform spectroscopy (in situ DRIFTS). The data were collected from 64 scans, with a resolution of 4 cm^{-1}. 50 mg of the catalyst were subjected to a pretreatment process at a temperature of 400 °C in an atmosphere comprising 10% H_2/Ar for a duration of one hour. This process was undertaken with the objective of eradicating impurities and moisture. Subsequently, the samples were exposed to an atmosphere comprising 2% NH_3 and Ar at a temperature of 50 °C for a

duration of 30 minutes. This was followed by desorption in an Ar atmosphere, with a heating rate from 50 °C to 350 °C.

The Raman scattering measurements were conducted using a Laboratory Human Resources Evolution Raman spectrometer (BX41). The catalysts were scanned within the range of 100-2000 cm-1 by means of the LabRam HR Evolution confocal microscope.

S3. Catalytic activity measurements

The NH_3 conversion rate was determined by means of continuous monitoring and analysis of the outlet gas composition. The conversion rate was calculated using the equation (1):

$$X_{NH_3} = \frac{C_{in} - C_{out}}{C_{in}} \times 100\% \quad (1)$$

In equation (1), X_{NH_3} is the ammonia conversion rate (%), C_{in} is the initial ammonia concentration entering the reactor (ppm), C_{out} is the ammonia concentration after passing through the catalyst (ppm). The H_2 generation rate is calculated using the equation (2):

$$r_{H_2} = \frac{\frac{V_{in}}{22.4} * X_{NH_3} * 1.5}{m_{cat}} \quad (2)$$

In equation (2), r_{H_2} is the rate of H_2 formation ($mmol \cdot g_{cat}^{-1} \cdot min^{-1}$), m_{cat} is the mass of the catalyst (g), and V_{in} is the amount of inlet obtained in the mass flow meter (L). The apparent activation energy and reaction rate of NH_3 decomposition were determined at NH_3 conversions below 20% and were calculated as in equation (3):

$$lnr = \frac{-E_a}{RT} + C \tag{3}$$

In equation (3), T denotes the reaction temperature (K), C denotes the constant term, E_a denotes the apparent activation energy (kJ·mol^{-1}), and r denotes the reaction rate (mol s^{-1} g^{-1}), which is calculated as in equation (4).

$$r = \frac{F \times [-\ln\left(\frac{1}{1-x}\right)]}{m_{cat}} \tag{4}$$

In equation (4), F represents the ammonia feed rate (mol·s^{-1}). E_a is obtained by the linear relationship between *lnr* and *1000/T* in the above equation

Turnover frequency (TOF), defined as the number of NH_3 molecules converted per active site per second, is calculated according to the equation:

$$TOF = \frac{F_{NH_3} \times X_{NH_3}}{x_a \times \frac{m_{cat}}{M_{cat}}} \tag{5}$$

In equation (5), $^{F_{NH_3}}$ denotes the flow rate of NH_3 (mol/s), $^{X_{NH_3}}$ represents the conversion rate of NH_3, m_{cat} indicates the mass of catalyst (g), M_{cat} denotes the malar of the catalysts (g/mol), and x_a signifies the reaction site in each sample.

Supplementary Results

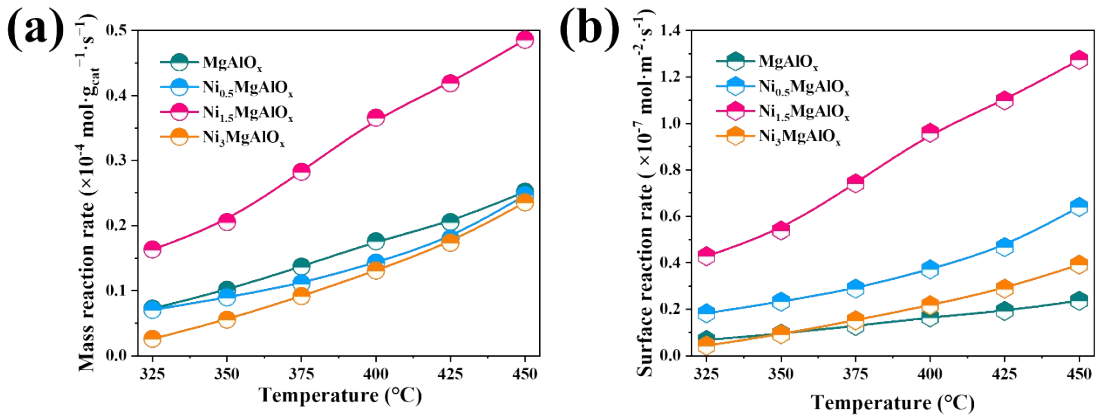

Figure S1. Mass reaction rate (a) and surface reaction rate (b) of Ni_aMgAlO_x catalyst at 325 - 450 °C.

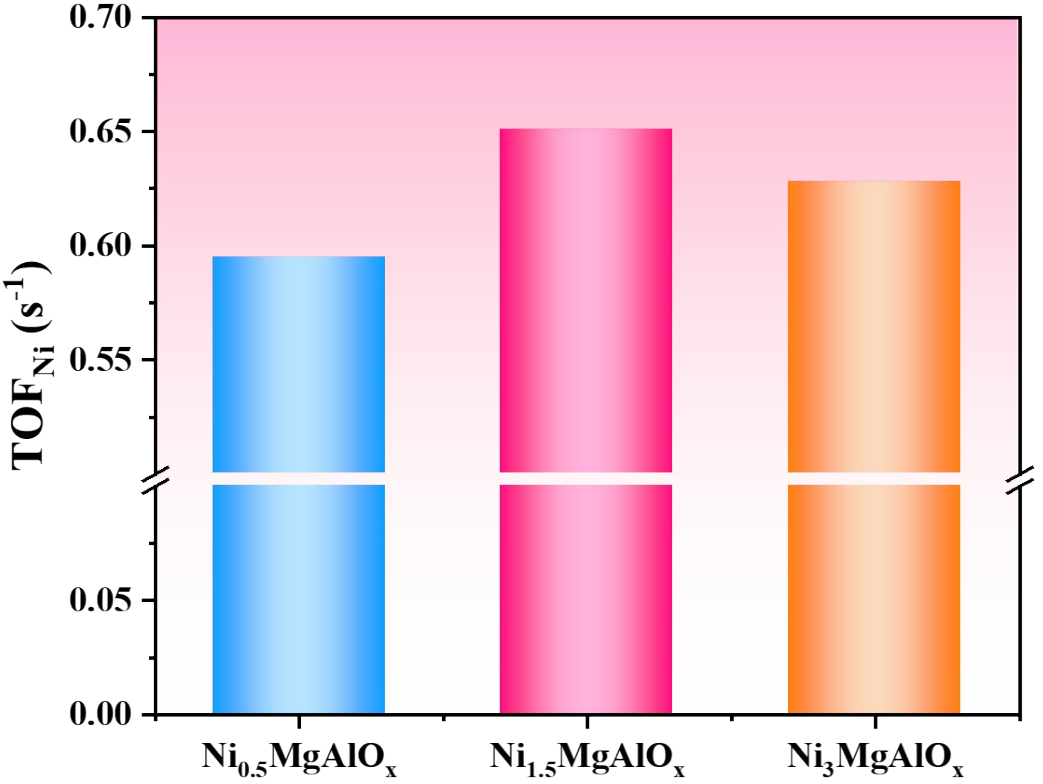

Figure S2. TOFs value of Ni_aMgAlO_x catalyst at 600 °C.

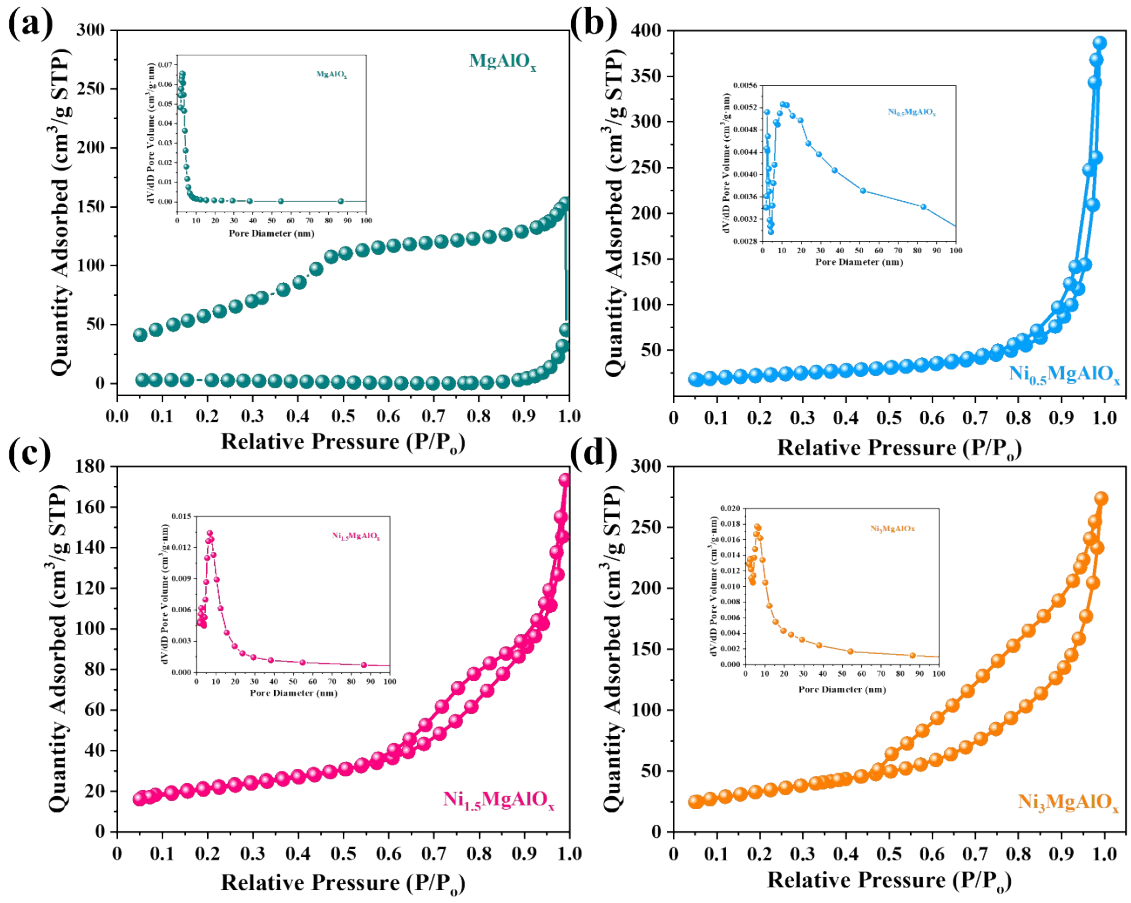

Figure S3. N_2 adsorption and desorption profiles of (a) $MgAlO_x$, (b) $Ni_{0.5}MgAlO_x$, (c) $Ni_{1.5}MgAlO_x$ and (d) Ni_3MgAlO_x.

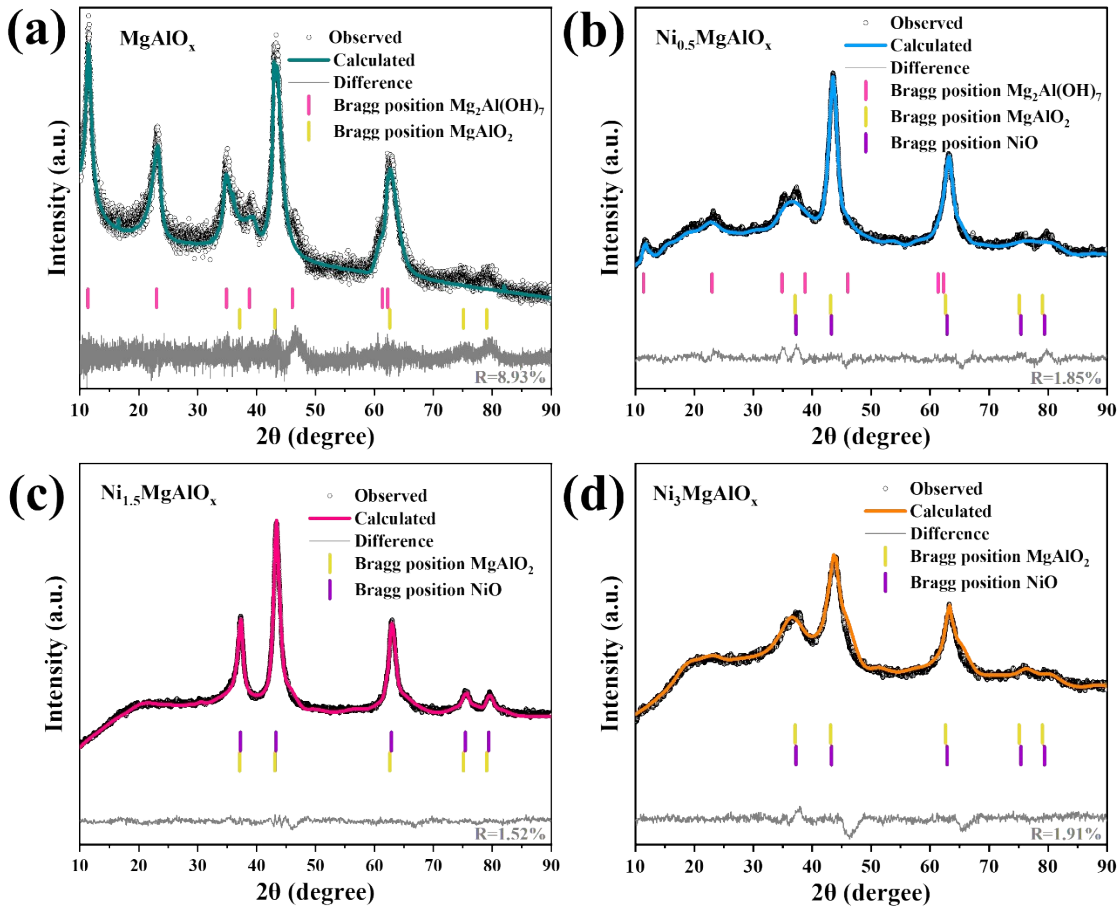

Figure S4. XRD spectra of Ni_aMgAlO_x samples. The calculated modes of the crystalline phases $Mg_2Al(OH)_7$ (PDF #48-0601), $MgAlO_2$ (PDF #24-0712) and NiO (PDF #47-1049) are shown below. Structural refinement plots of powder diffraction data for (a) $MgAlO_x$, (b) $Ni_{0.5}MgAlO_x$, (c) $Ni_{1.5}MgAlO_x$, and (d) Ni_3MgAlO_x at room temperature. The plots also show the observed (black circles), calculated (coloured solid lines) and difference (grey solid lines) intensities, and calculated Bragg reflections (ticked).

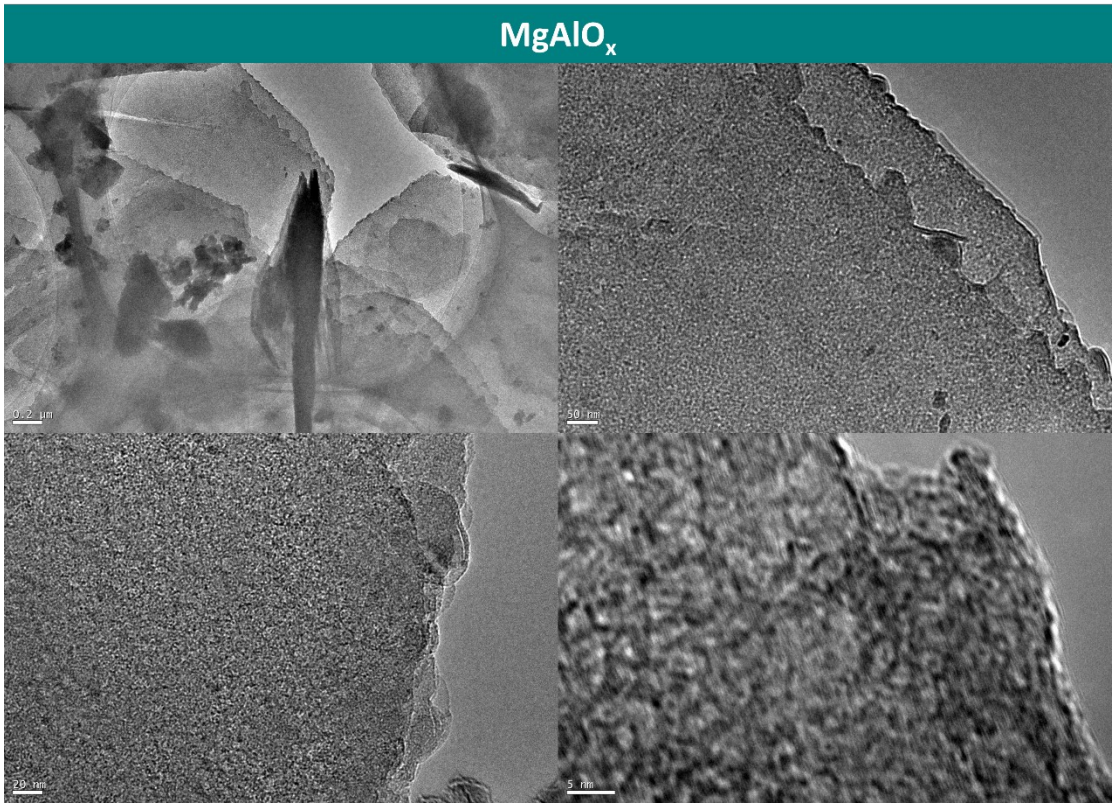

Figure S5. TEM image of $MgAlO_x$ catalyst.

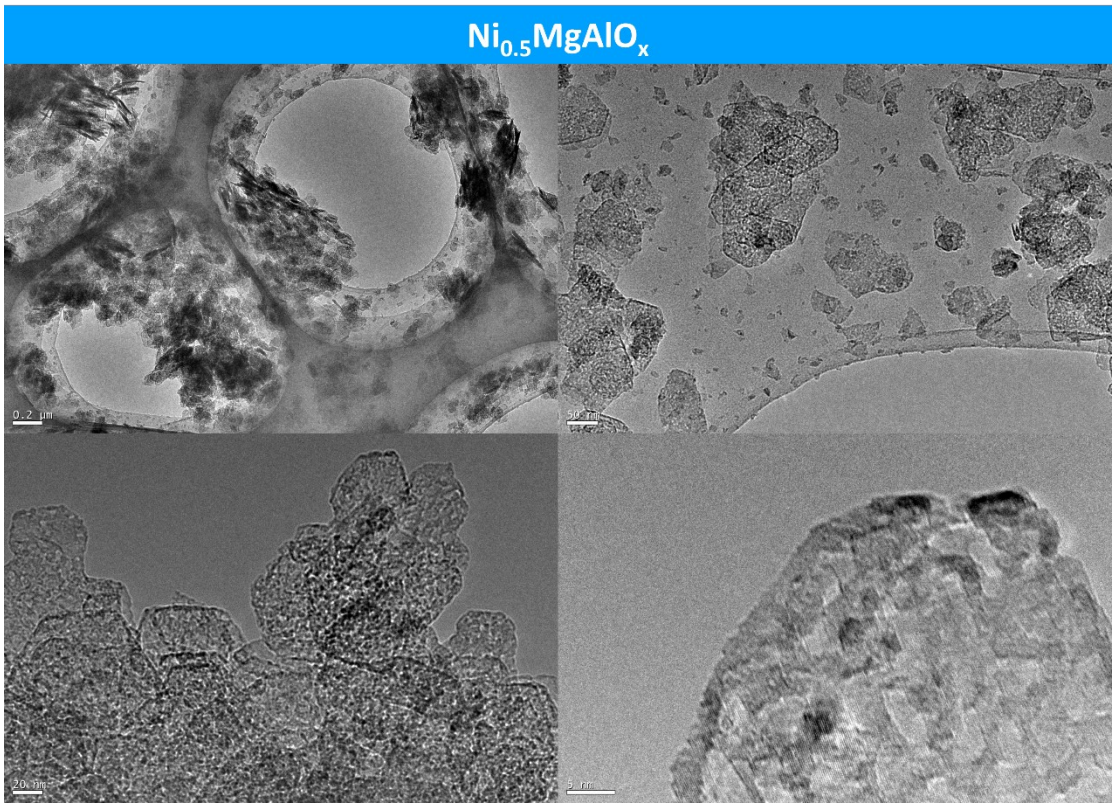

Figure S6. TEM image of $Ni_{0.5}MgAlO_x$ catalyst.

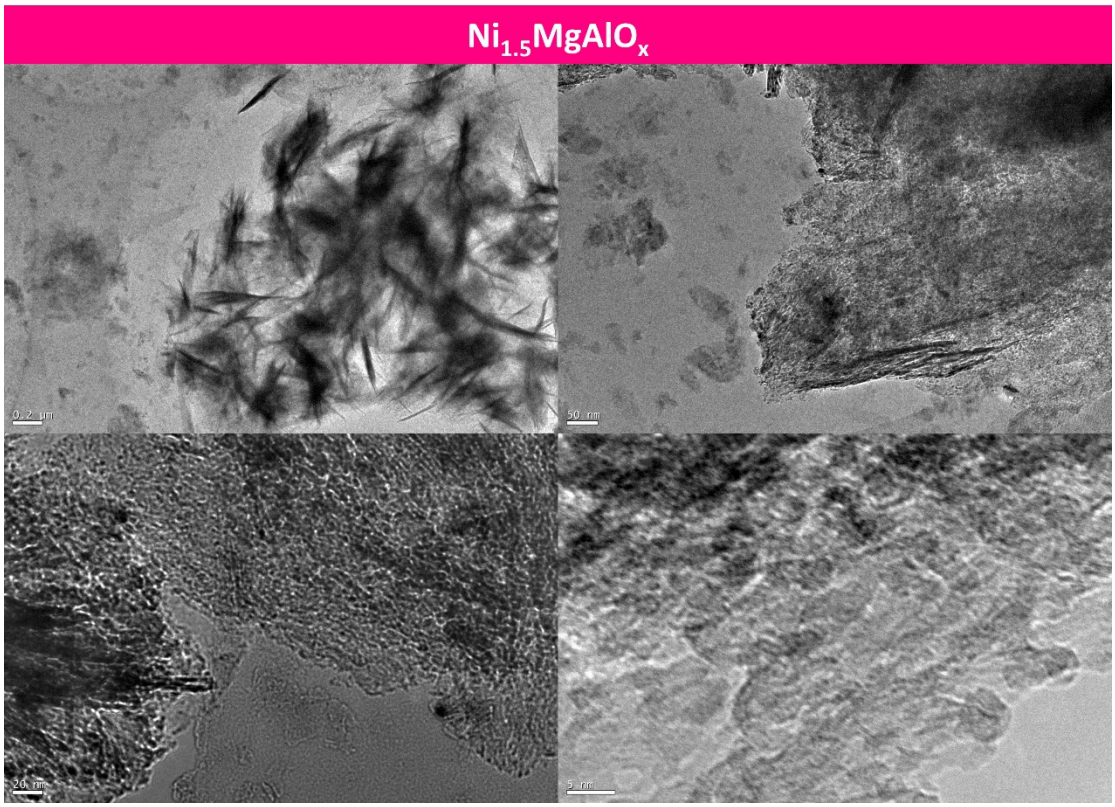

Figure S7. TEM image of $Ni_{1.5}MgAlO_x$ catalyst.

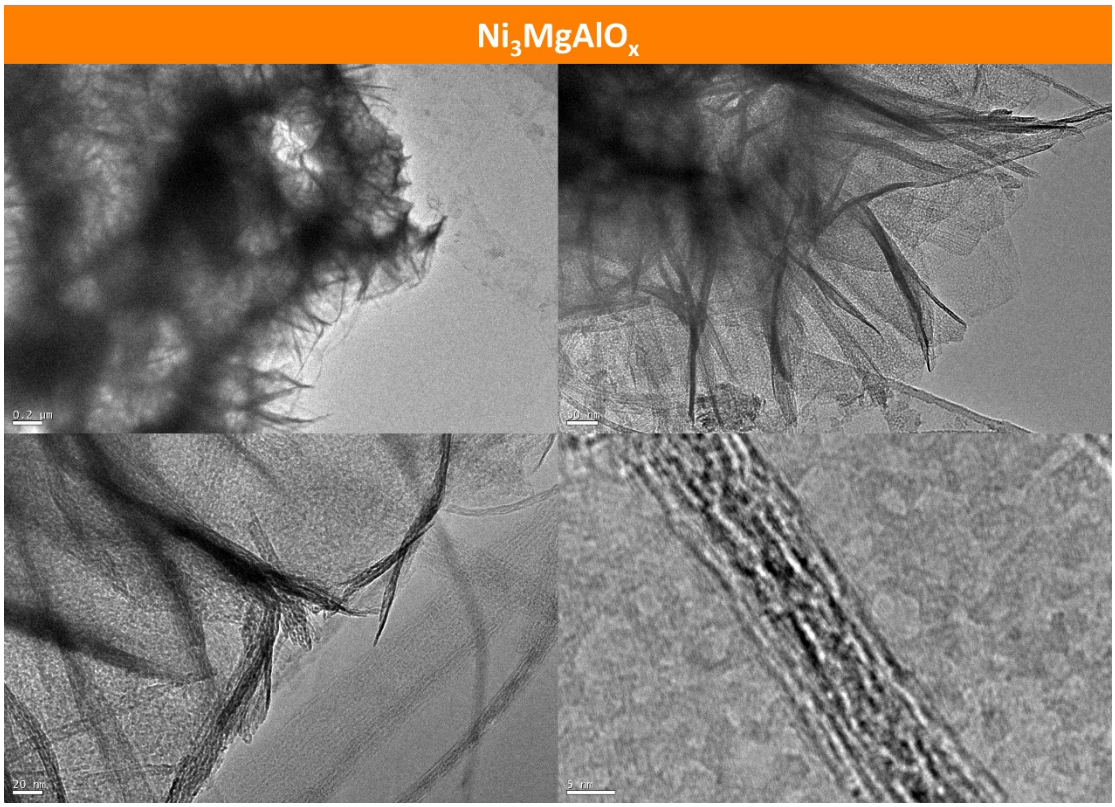

Figure S8. TEM image of Ni_3MgAlO_x catalyst.

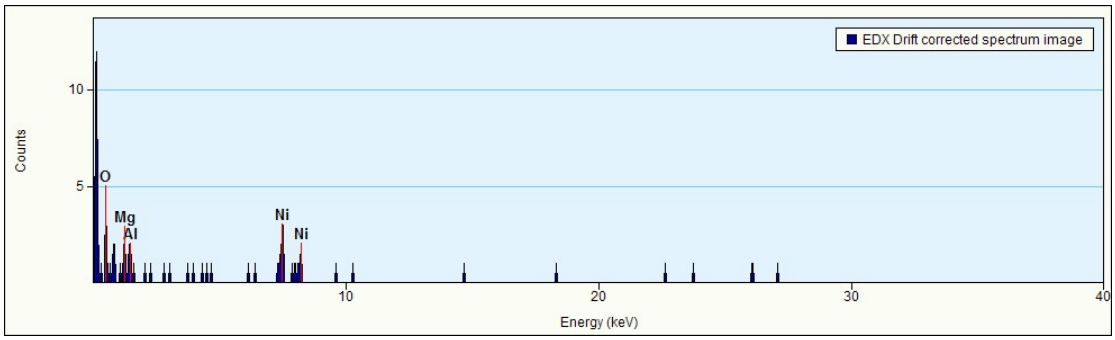

Figure S9. EDX drift corrected spectrum image display.

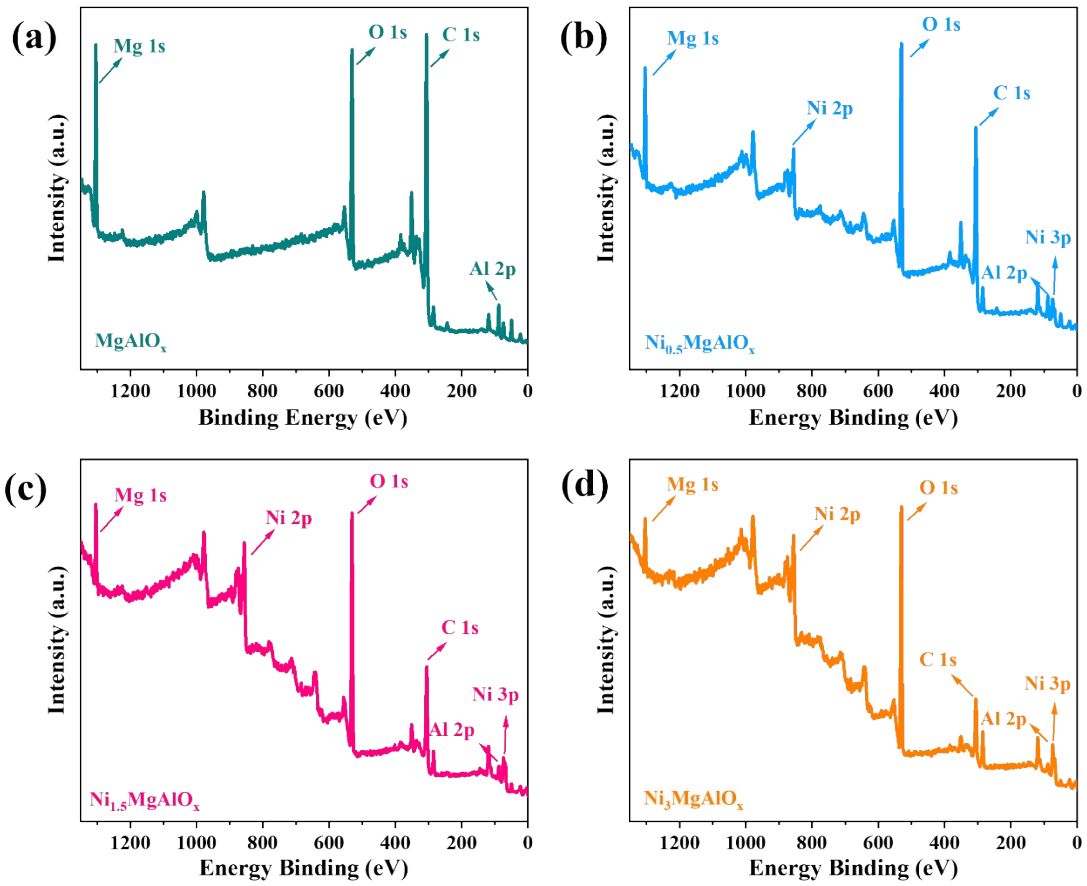

Figure S10. XPS full spectrum analysis of (a) $MgAlO_x$, (b) $Ni_{0.5}MgAlO_x$, (c) $Ni_{1.5}MgAlO_x$ and (d) Ni_3MgAlO_x catalysts.

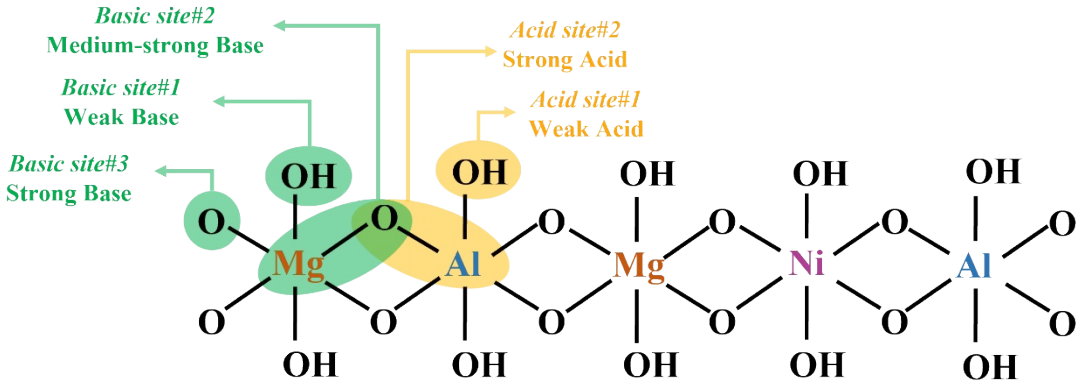

Figure S11. Schematic diagram of the acid and base site structure of Ni_aMgAlO_x.

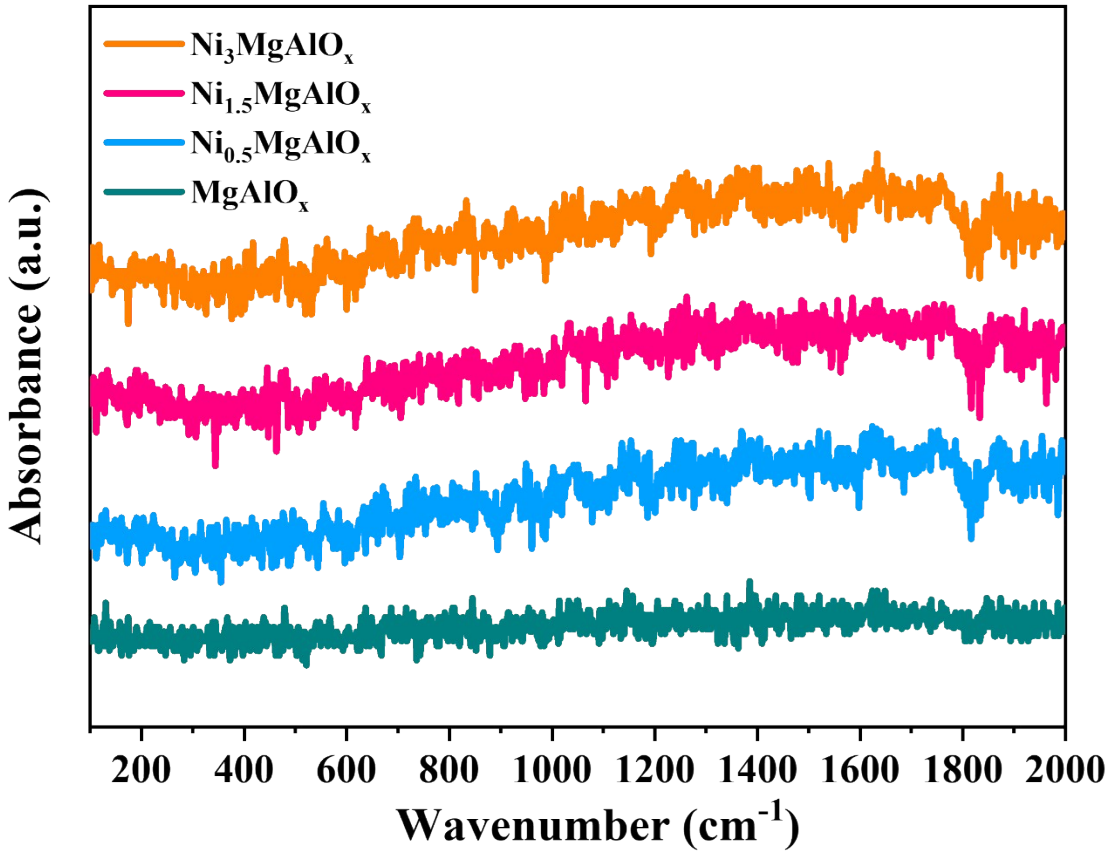

Figure S12. Raman spectra of Ni_aMgAlO_x catalysts.

Table S1. The peak area of different base sites determined by CO_2-TPD profile.

Sample	Weak base		Medium-strong base				Strong base						Total base
	position	area	position	area	position	area	position	area	position	area	position	area	
$MgAlO_x$	103.2	27.7	194	126	-	-	388.3	290.2	505.9	665.2	-	-	1109.1
$Ni_{0.5}MgAlO_x$	103.5	26.3	191	173.8	-	-	396	164	514.6	469.2	-	-	833.3
$Ni_{1.5}MgAlO_x$	100.3	16.4	162.5	31.9	316.2	27.3	402.2	107.1	596.8	246.5	-	-	429.2
Ni_3MgAlO_x	98.9	23.6	168.7	125.6	-	-	380.8	130.6	469.4	272.6	646.9	354.3	906.7

Table S2. The peak area of different acid sites determined by NH_3-TPD profile.

Sample	Weak acid		Strong acid				Total acid
	position	area	position	area	position	area	
$MgAlO_x$	101.2	12.4	510.8	65.7	-	-	78.1
$Ni_{0.5}MgAlO_x$	101.3	15.9	374.6	33.6	-	-	49.5
$Ni_{1.5}MgAlO_x$	117.3	8.2	523	93.6	639.3	40.5	142.3
Ni_3MgAlO_x	100.2	16.7	-	-	735.9	120	136.7

Table S3. Fitted parameters for **Ni 2p** XPS spectra.

Sample	Assignment	Binding Energy (eV)	FWHM (eV)	Peak Area (a.u.)	Area (%)
$Ni_{0.5}MgAlO_x$	$Ni^0(2p_{3/2}$ Main)	853.80	3.53	735.95	2.31
	$Ni^{2+}(2p_{3/2}$ Main)	855.50	3.42	11152.80	34.98
	Satellite ($2p_{3/2}$)	860.50	3.62	10371.42	32.53
	$Ni^0(2p_{1/2}$ Main)	870.50	5.81	1300.14	4.08
	$Ni^{2+}(2p_{1/2}$ Main)	872.90	3.31	4047.93	12.70
	Satellite ($2p_{1/2}$)	879.00	3.45	4274.85	13.41
$Ni_{1.5}MgAlO_x$	$Ni^0(2p_{3/2}$ Main)	853.00	3.41	2263.76	4.90
	$Ni^{2+}(2p_{3/2}$ Main)	854.96	3.01	13511.64	29.25
	Satellite ($2p_{3/2}$)	860.61	4.02	12828.79	27.78
	$Ni^0(2p_{1/2}$ Main)	870.40	2.17	1483.64	3.21
	$Ni^{2+}(2p_{1/2}$ Main)	872.49	3.27	9002.93	19.49
	Satellite ($2p_{1/2}$)	879.10	4.45	7095.38	15.36
Ni_3MgAlO_x	$Ni^0(2p_{3/2}$ Main)	852.81	3.36	1507.84	3.12
	$Ni^{2+}(2p_{3/2}$ Main)	854.90	2.77	17164.88	35.56
	Satellite ($2p_{3/2}$)	861.14	3.51	12195.72	25.26
	$Ni^0(2p_{1/2}$ Main)	870.40	3.23	707.27	1.47
	$Ni^{2+}(2p_{1/2}$ Main)	872.38	3.19	11864.90	24.58
	Satellite ($2p_{1/2}$)	879.47	3.42	4832.42	10.01

Table S4. Fitted parameters for **O 1s**, **Mg 1s** and **Al 2p** XPS spectra.

Sample	Assignment	FWHM (eV)	Binding Energy (eV)	Peak Area (a.u.)	Area (%)
$MgAlO_x$	O_{lat}	2.33	529.80	27616.55	69.86
	O_{ads}	2.03	531.50	11912.22	30.14
	MgO	2.13	1304.33	36035.24	68.85
	$Mg(OH)_2$	1.67	1303.33	16301.67	31.15
	Al^{3+}	1.98	73.93	2414.88	100.00
$Ni_{0.5}MgAlO_x$	O_{lat}	2.19	529.80	42021.68	76.18
	O_{ads}	1.73	531.50	13141.99	23.82
	MgO	1.95	1304.13	26680.91	53.15
	$Mg(OH)_2$	1.91	1303.23	23517.96	46.85
	Al^{3+}	1.97	73.78	4617.31	100.00
$Ni_{1.5}MgAlO_x$	O_{lat}	2.28	529.80	26275.98	74.92
	O_{ads}	1.9	531.50	8798.16	25.08
	MgO	2.09	1304.33	10833.55	48.25
	$Mg(OH)_2$	1.97	1303.43	11617.74	51.75
	Al^{3+}	2.13	73.73	3430.63	100.00
Ni_3MgAlO_x	O_{lat}	2.52	529.80	19396.53	74.36
	O_{ads}	1.90	531.50	6687.32	25.64
	MgO	2.09	1304.23	6003.75	54.85
	$Mg(OH)_2$	3.58	1303.33	4941.30	45.15
	Al^{3+}	1.96	73.83	2193.88	100.00

Table S5. Activation energy and reaction rate of Ni_aMgAlO_x catalyst.

Sample	T_{50} (°C)	Ea (kJ·mol^{-1})	r (×10^{-5} mol·g^{-1}·s^{-1})	Ln(r) (mmol·g_{cat}^{-1}·min^{-1})	R^2
$MgAlO_x$	534.99	35.60	15.86	-8.75	0.991
$Ni_{0.5}MgAlO_x$	519.16	35.29	12.54	-8.98	0.986
$Ni_{1.5}MgAlO_x$	498.37	24.23	16.26	-8.72	0.992
Ni_3MgAlO_x	522.37	61.55	21.61	-8.44	0.972

Reference

[1]. Q. Su, L. Gu, Y. Yao, J. Zhao, W. Ji, W. Ding, C.-T. Au, Layered double hydroxides derived $Ni_x(Mg_yAl_zO_n)$ catalysts: Enhanced ammonia decomposition by hydrogen spillover effect, Applied Catalysis B: Environmental, 201 (2017) 451-460.

[2]. Q.C. Do, Y. Kim, T.A. Le, G.J. Kim, J.-R. Kim, T.-W. Kim, Y.-J. Lee, H.-J. Chae, Facile one-pot synthesis of Ni-based catalysts by cation-anion double hydrolysis method as highly active Ru-free catalysts for green H_2 production via NH_3 decomposition, Applied Catalysis B: Environment and Energy, 307 (2022) 121167.

[3]. J. Shin, U. Jung, J. Kim, K.D. Kim, D. Song, Y. Park, B.-S. An, K.Y. Koo, Elucidating the effect of Ce with abundant surface oxygen vacancies on $MgAl_2O_4$-supported Ru-based catalysts for ammonia decomposition, Applied Catalysis B: Environmental, 340 (2024) 123234.

[4]. T.H. Ulucan, J. Wang, E. Onur, S. Chen, M. Behrens, C. Weidenthaler, Unveiling the Structure-Property Relationship of MgO-Supported Ni Ammonia Decomposition Catalysts from Bulk to Atomic Structure by In Situ/Operando Studies, ACS Catalysis, 14 (2024) 2828-2841.

[5]. Z. Zhao, Z. Liu, M. Li, Y. Yang, L. Deng, Y. Zhao, B. Dou, F. Bin, Enhancing ammonia decomposition for hydrogen production via optimization of interface effects and acidic site in supported cobalt-nickel alloy catalysts, Separation and Purification Technology, 360 (2025) 131144.

[6] Y. Yan, W. Zhu, J. Wang, Y. Li, C. Zhao, C. Liang, MgAl-LDH derived oxides supported Ni catalysts: Tuning acidity-basicity for enhanced ammonia decomposition, Int. J. Hydrogen Energy 164 (2025) 150855.